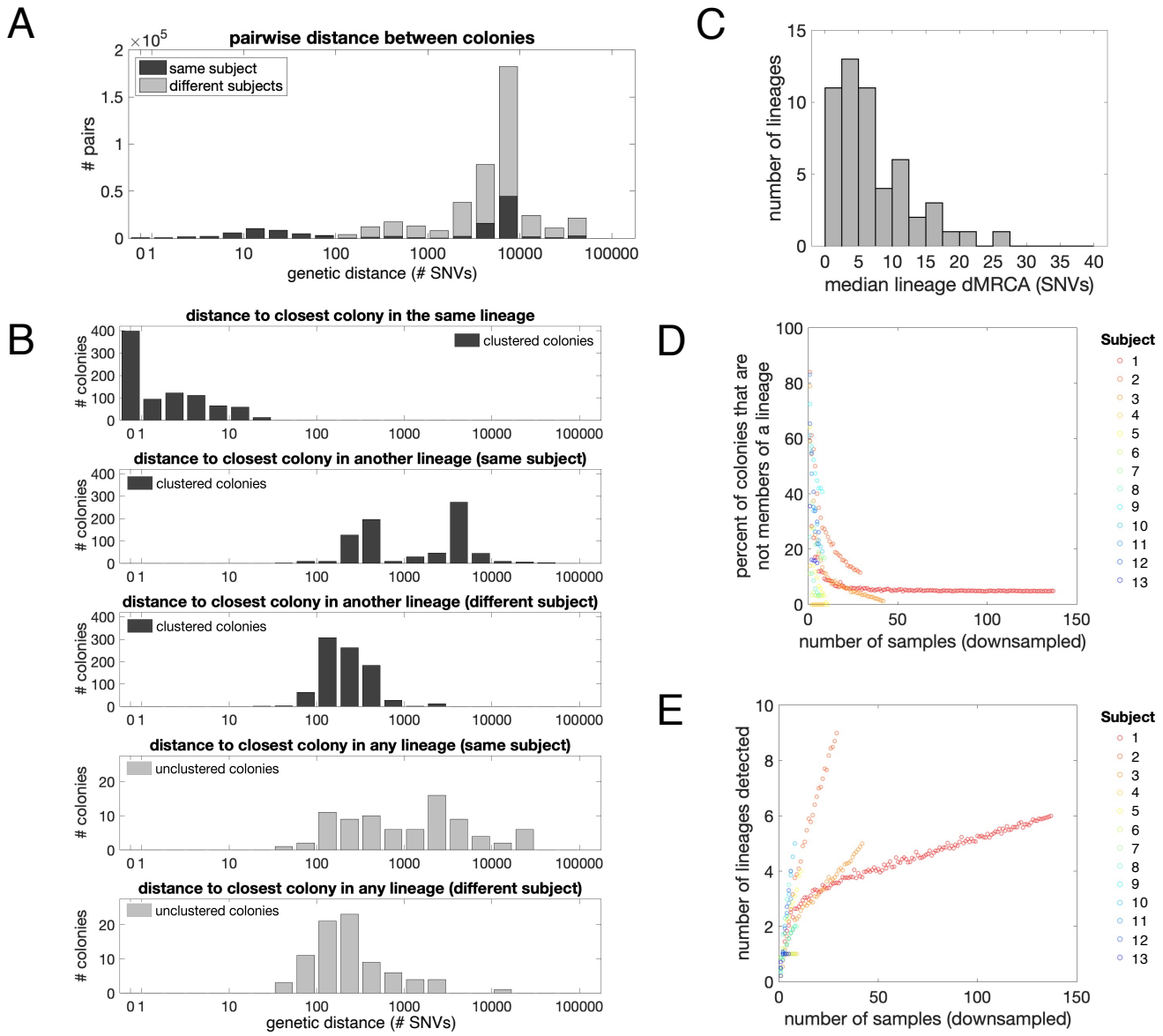

Figure S1. Clustering distance thresholds and collector's curves, related to Figure 1 and STAR Methods. (A) Histogram of the genetic distance (in single nucleotide variants) between pairs of colonies from the same subject vs different subjects. The bimodal distribution for same-subject pairs reflects that *C. acnes* genotypes found on an individual cluster into closely related lineages. (B) Histograms of the distance (in single nucleotide variants) to the nearest colony from various sets (see subpanel titles). The top three histograms consider clustered colonies (dark gray), while the bottom two histograms consider unclustered colonies (light gray). The minimum distance from a clustered colony to a lineage on another subject is generally lower than the minimum distance to another lineage on the same subject because the set of colonies belonging to other subjects is larger and thus contains representatives from a broader selection of strain types. In (C), we plot a histogram of the median distance between a lineage's inferred ancestor and the colonies belonging to that lineage. For each subject, we show collector's curves for (D) the percent of colonies that do not cluster with any lineage and (E) the number of lineages detected. Each dot represents the average over 100 downsampled sets; we downsample samples rather than colonies, as colonies from the same sample are more likely to be from the same lineage. We note 3 colonies are required to define a lineage, which results in a collector's curve with a steeper tail (E) than in a traditional collector's curve. The lack of saturation reflects the presence of low-abundance lineages and demonstrates the difficulty in estimating the true number of resident lineages.

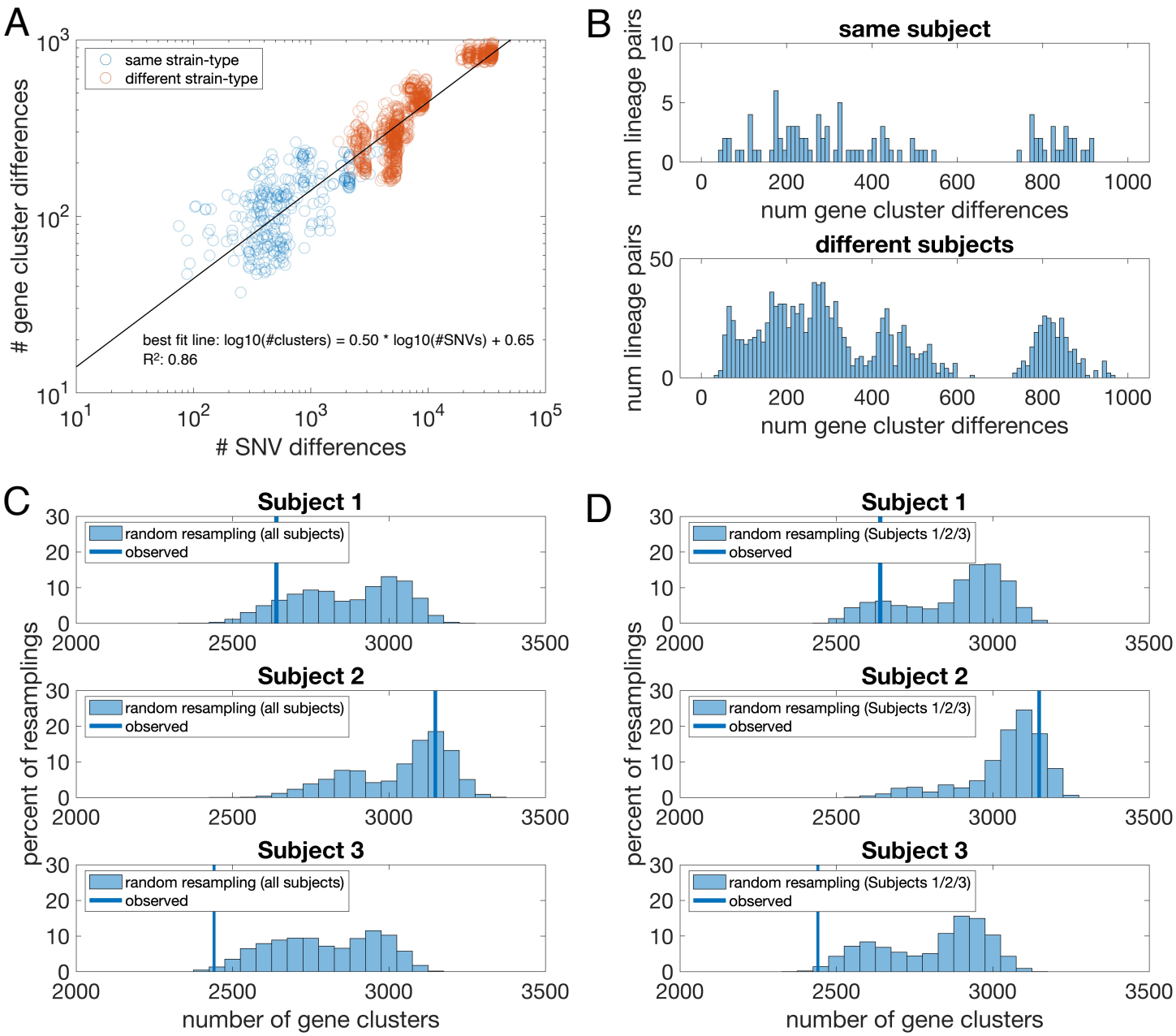

Figure S2. Coexisting lineages on the same subject are not enriched for gene content differences, related to Figure 2. (A) We quantified gene content differences between lineages by clustering genes in lineage assembled genomes and then finding the number of gene cluster differences between pairs of lineages (i.e. the number of gene clusters present in one but not both members of a pair). As expected for a species with low rates of gene transfer (Tomida et. al., 2013), the number of gene cluster differences between pairs of lineages was strongly related to the number of SNVs across the core genome (R^2=0.86). (B) The number of gene cluster differences between pairs of lineages on the same subject did not differ from the number of gene cluster differences between pairs of lineages on different subjects (ks test, P=0.7). Furthermore, we find many pairs of lineages that coexist on the same subject that have similar gene content, suggesting that differences in gene content are not required for coexistence. (C) Additionally, the number of gene clusters present across all lineages detected on an individual person is not significantly enriched relative to the number of gene clusters present among a random resampling of the same number of lineages randomly drawn from our dataset (P=0.85, 0.20, 0.99 respectively). This analysis includes all subjects from whom we have at least 25 samples with colonies that passed quality filters. (D) Same as (C), but resampling lineages from Subjects 1, 2, and 3 only (P=0.84, 0.09, 0.99 respectively).

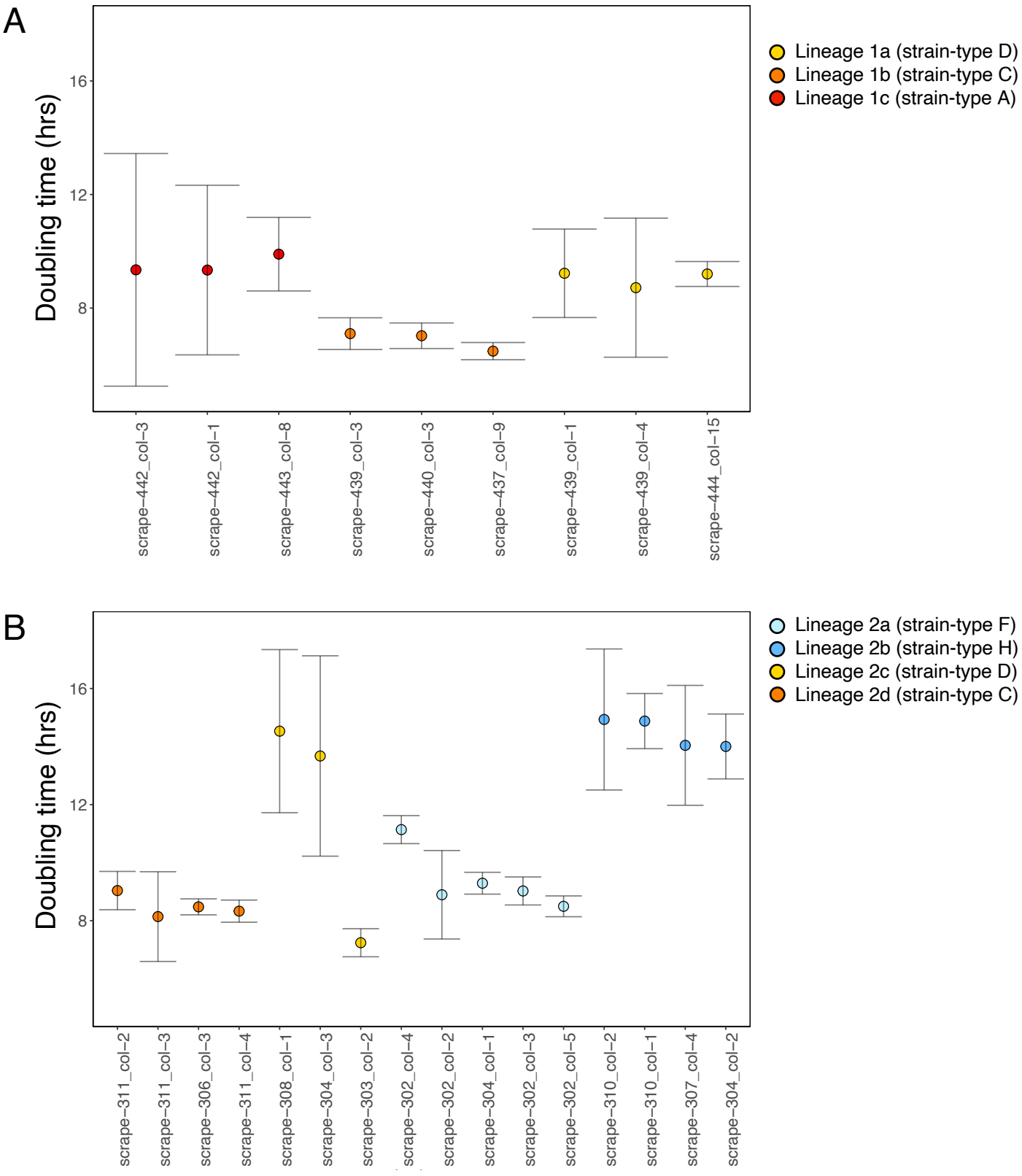

Figure S3. Co-existing *C. acnes* genotypes have different doubling times *in vitro*, related to Figure 2. Each dot represents the mean observed doubling time among replicates for a given isolate (Methods), and error bars represent 95% CIs of the mean doubling time for each isolate (+/- 1.97 SEM). There were 3 replicates for each Subject 1 isolate (A) and 4 replicates for each Subject 2 isolate (B). Color indicates phylogenetic grouping by lineage. The isolates do not all have the same doubling time (one way ANOVA, $P = 2.7\times10^{-4}$ for Subject 1 and $P = 2.2\times10^{-16}$ for Subject 2).

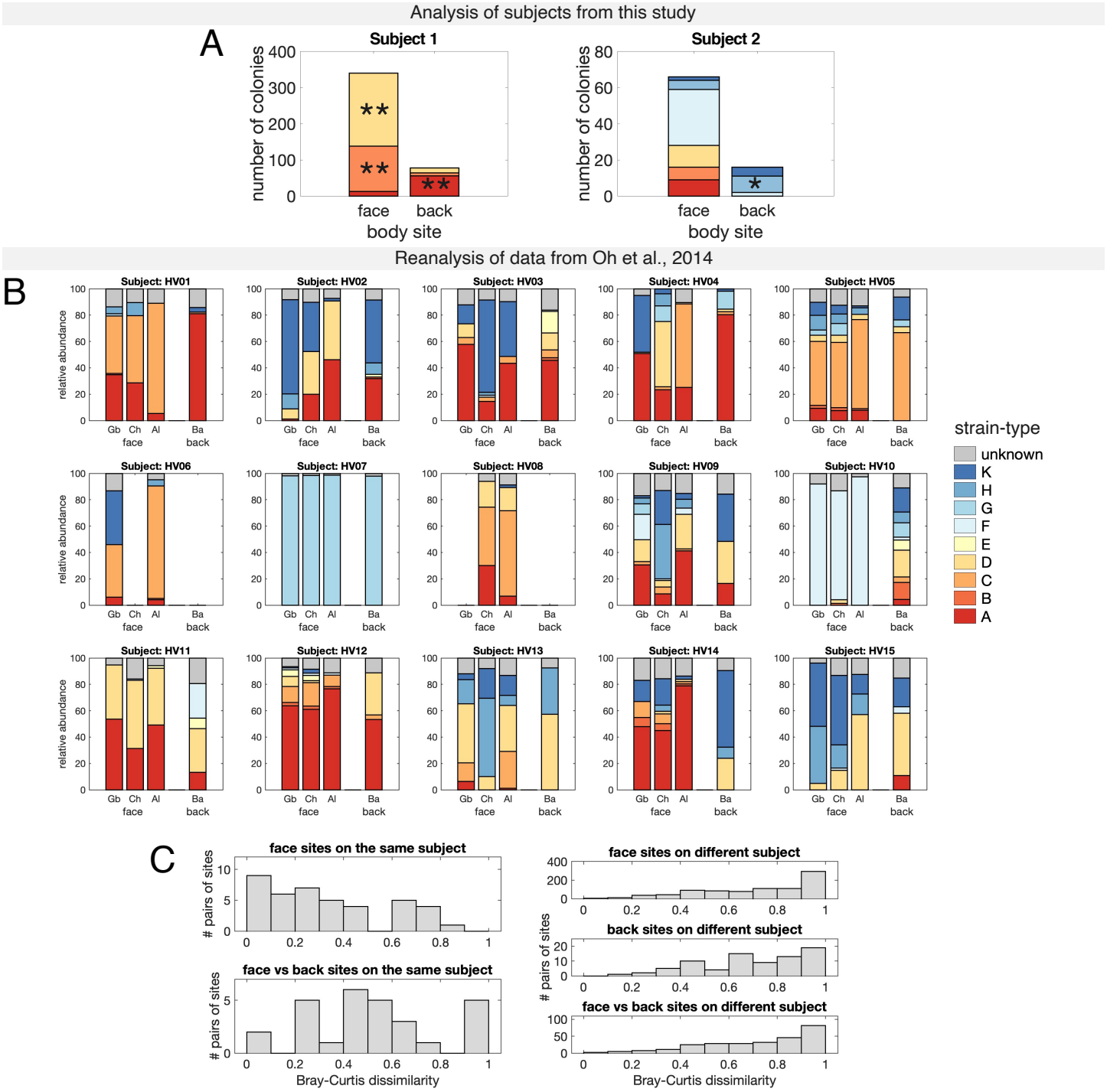

Figure S4. Different strain enrichment patterns on the face vs the back on some subjects suggest a priority effect, related to Figure 3. (A) Bar charts showing the number of colonies belonging to each strain type on the face vs back for subjects with at least 10 colonies on each site. Some strains are enriched on the face vs the back (*P<0.01, **P<0.001, binomial test with Bonferroni correction). (B,C) Reanalysis of published data by grouping relative abundances (from Supplemental Table 11 in Oh et al., 2014) at the strain-type level. Variation between face sites (Gb = glabella, Ch = cheek, Al = alar crease) and the back (Ba) differs between individual subjects. (C) Face sites on the same subject are more similar to each other than they are to the back (Bray-Curtis dissimilarity of strain type relative abundance; Wilcoxon rank-sum test, P<0.01). However, back sites on different subjects and face sites on different subjects are not significantly more similar than face vs back sites on different subjects (Wilcoxon rank sum test). Since enrichment patterns are not conserved across subjects, these findings support a priority effect rather than generic back-adapted or face-adapted strains.

A

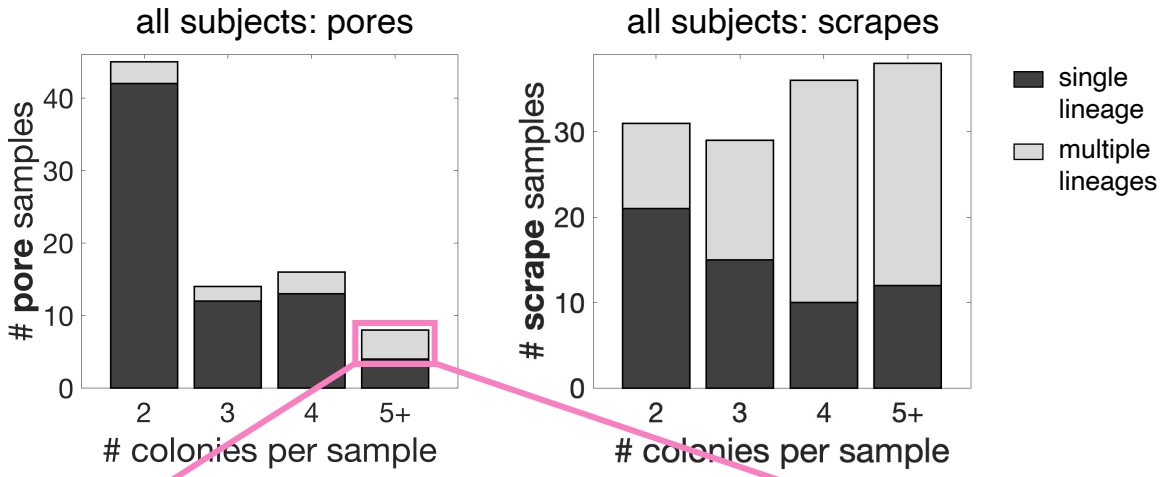

B

Pore sample number	Lineage	Strain-type	Portion of colonies
44	1a	D	3/5
	1b	C	2/5
395	5c	A	4/6
	5a	D	1/6
	5d	A	1/6
406	8d	K	4/6
	8a	D	2/6
407	8a	D	4/5
	8b	H	1/5

Figure S5. Lineage diversity in pore vs scrape samples, related to Figure 3. (A) The enrichment of single lineages within individual pores persists across all subjects. Colonies from the same pore sample typically belong to the same lineage (left), whereas colonies from the same coarse scrape samples often belong to more than one lineage (right). (B) Summary of pore samples with at least 5 colonies that do not all originate from the same lineage. In all cases, multiple lineages found in the same pore represent multiple strain-types; this argues against selection for a specific strain-type within a given pore.

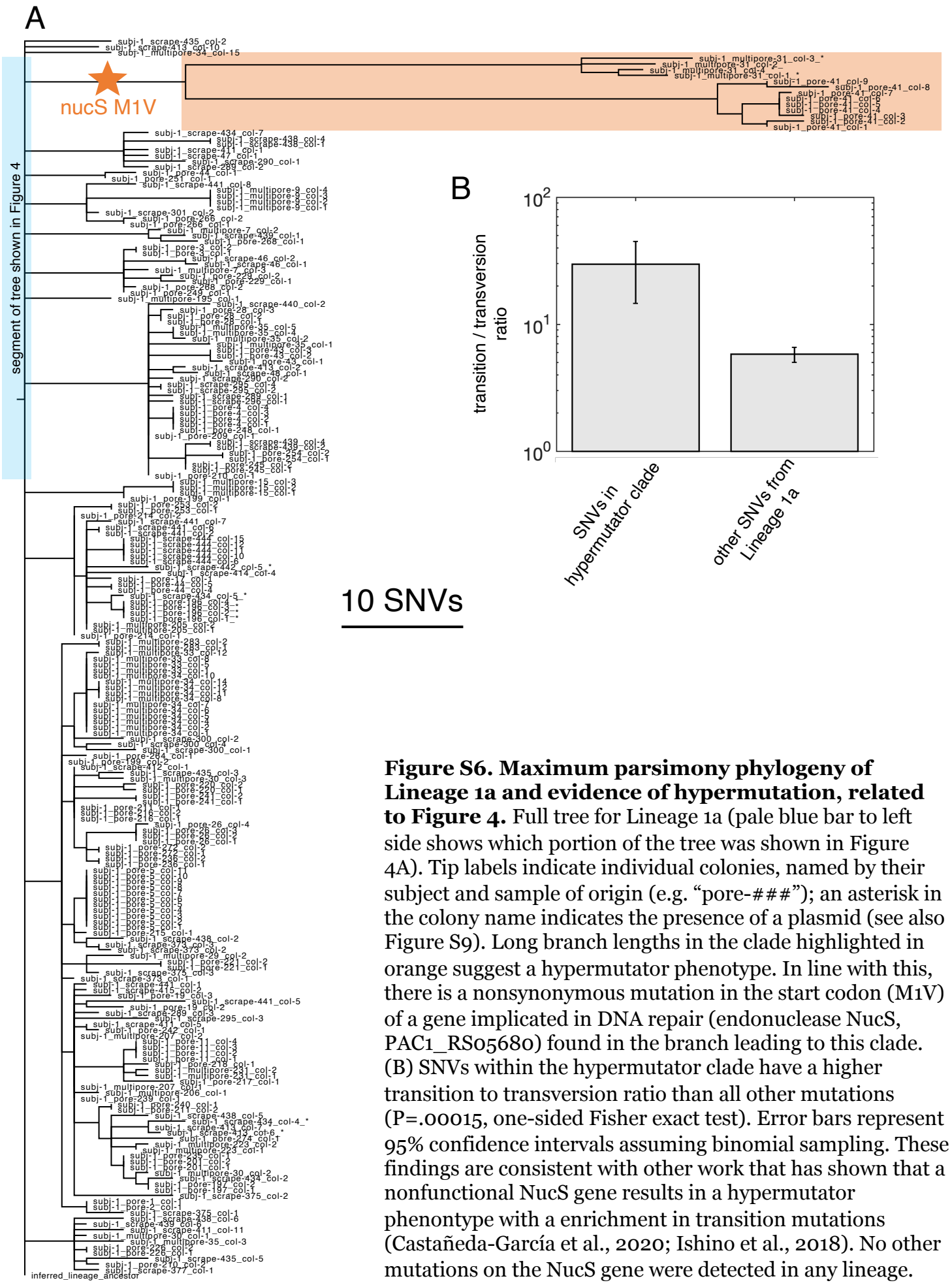

Figure S6. Maximum parsimony phylogeny of Lineage 1a and evidence of hypermutation, related to Figure 4. Full tree for Lineage 1a (pale blue bar to left side shows which portion of the tree was shown in Figure 4A). Tip labels indicate individual colonies, named by their subject and sample of origin (e.g. "pore-###"); an asterisk in the colony name indicates the presence of a plasmid (see also Figure S9). Long branch lengths in the clade highlighted in orange suggest a hypermutator phenotype. In line with this, there is a nonsynonymous mutation in the start codon (M1V) of a gene implicated in DNA repair (endonuclease NucS, PAC1_RS05680) found in the branch leading to this clade. (B) SNVs within the hypermutator clade have a higher transition to transversion ratio than all other mutations (P=.00015, one-sided Fisher exact test). Error bars represent 95% confidence intervals assuming binomial sampling. These findings are consistent with other work that has shown that a nonfunctional NucS gene results in a hypermutator phenontype with a enrichment in transition mutations (Castañeda-García et al., 2020; Ishino et al., 2018). No other mutations on the NucS gene were detected in any lineage.

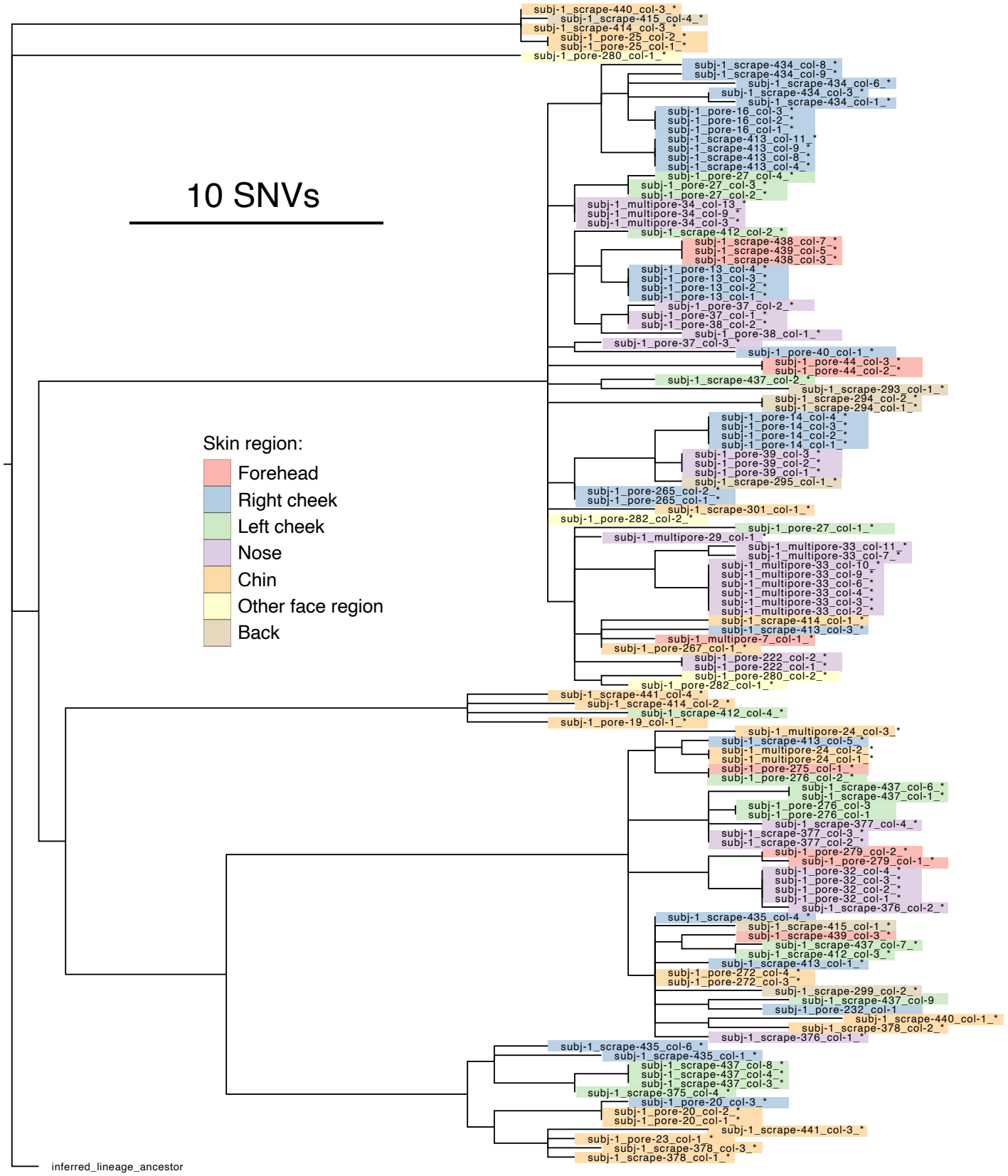

Figure S7. Maximum parsimony phylogeny of Lineage 1b, related to Figure 4. Full lineage tree of the second most abundant lineage on Subject 1, which also shows a pattern of low diversity within pores and pore-specific genotypes. Tip labels indicate individual colonies, named by their subject and sample of origin (e.g. "pore-###"); an asterisk at the end of the colony name indicates the presence of a plasmid (see Figure S9). Highlight colors indicate skin region and show that closely related genotypes are not necessarily co-localized. Long branches leading to subclades might reflect the transmission of multiple closely related genotypes to Subject 1 from a single source (e.g. a parent), or an expansion of particular genotypes following colonization (neutral or adaptive expansion).

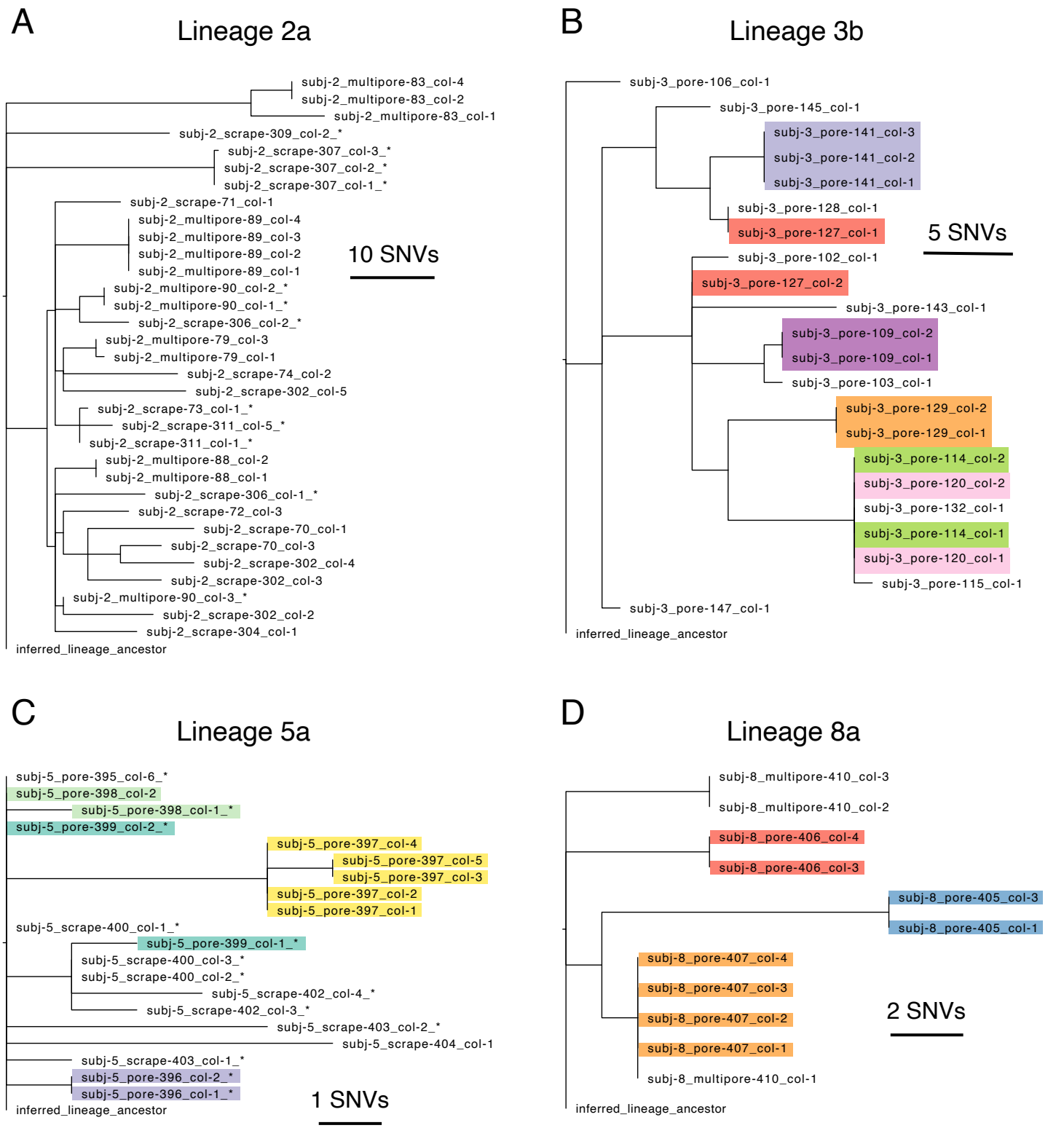

Figure S8. Maximum parsimony trees of other lineages with pore samples from four different subjects, related to Figure 4. These are the four largest lineages containing pore samples from four distinct subjects (excluding Lineages 1a, 1b, and 3a which have already been shown in Figures 4, S6, and S7). Colonies are colored by pore (excluding multipore samples and pore samples with only one colony), emphasizing low within-pore diversity and pore-specific genotypes. We note that Lineage 2a contains many multipore samples (extractions that appeared to have perturbed more than one follicle); although colonies originating from these samples are often monophyletic, we have opted not to highlight them. Tip labels indicate individual colonies, named by their subject and sample of origin; asterisks in the colony name indicate the presence of a plasmid (see Figure S9).

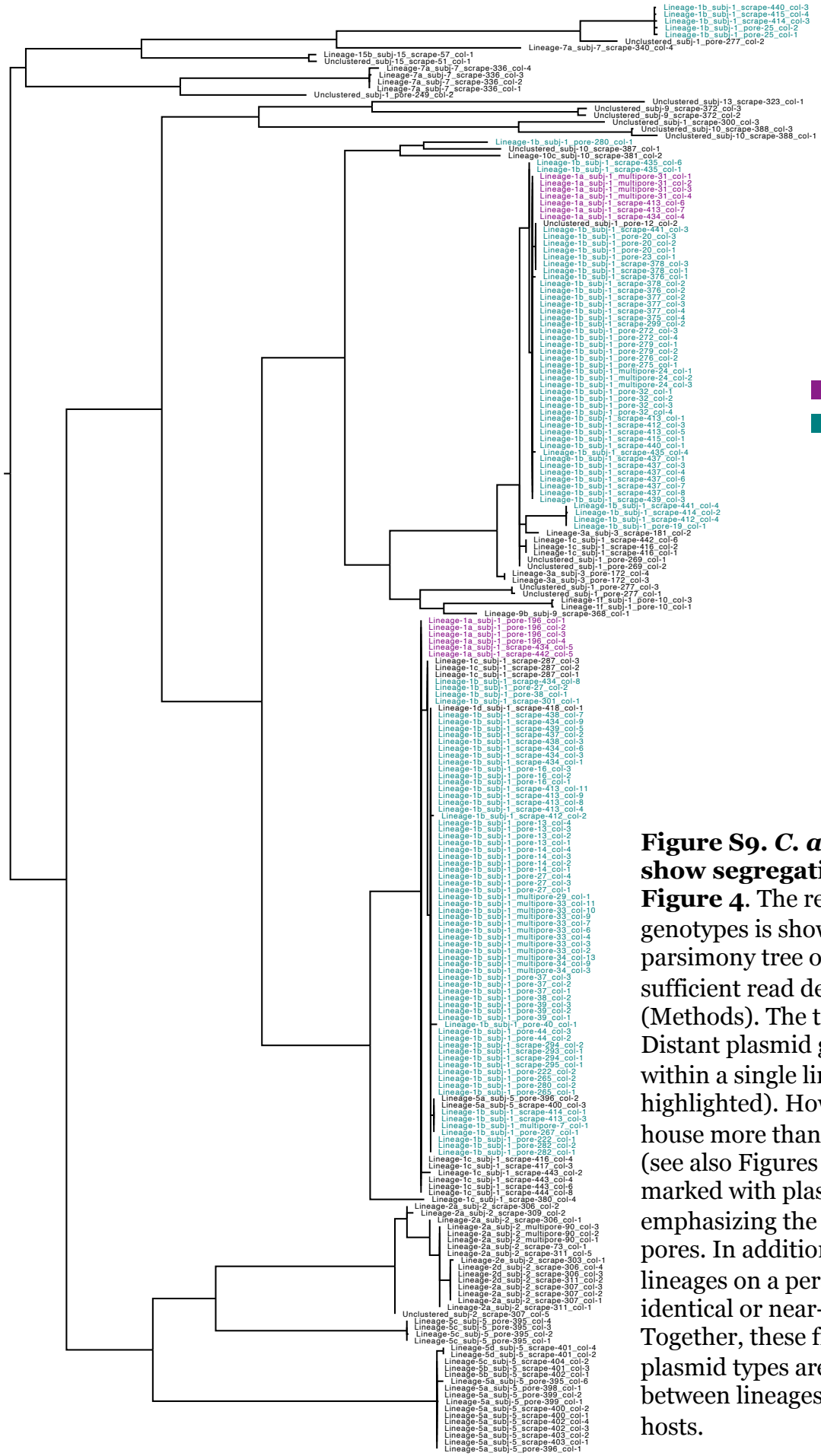

Figure S9. *C. acnes* plasmids also show segregation by pore, related to Figure 4. The relationship of plasmid genotypes is shown as a maximum parsimony tree of variable positions with sufficient read depth across samples (Methods). The tree is midpoint-rooted. Distant plasmid genotypes can be found within a single lineage (Lineages 1a and 1b highlighted). However, single pores never house more than one plasmid genotype (see also Figures S6-8 for lineage trees marked with plasmid presence), emphasizing the island-like nature of pores. In addition, colonies from different lineages on a person share plasmids with identical or near-identical genotypes. Together, these findings indicate that new plasmid types are gained, transferred between lineages, and lost on individual hosts.

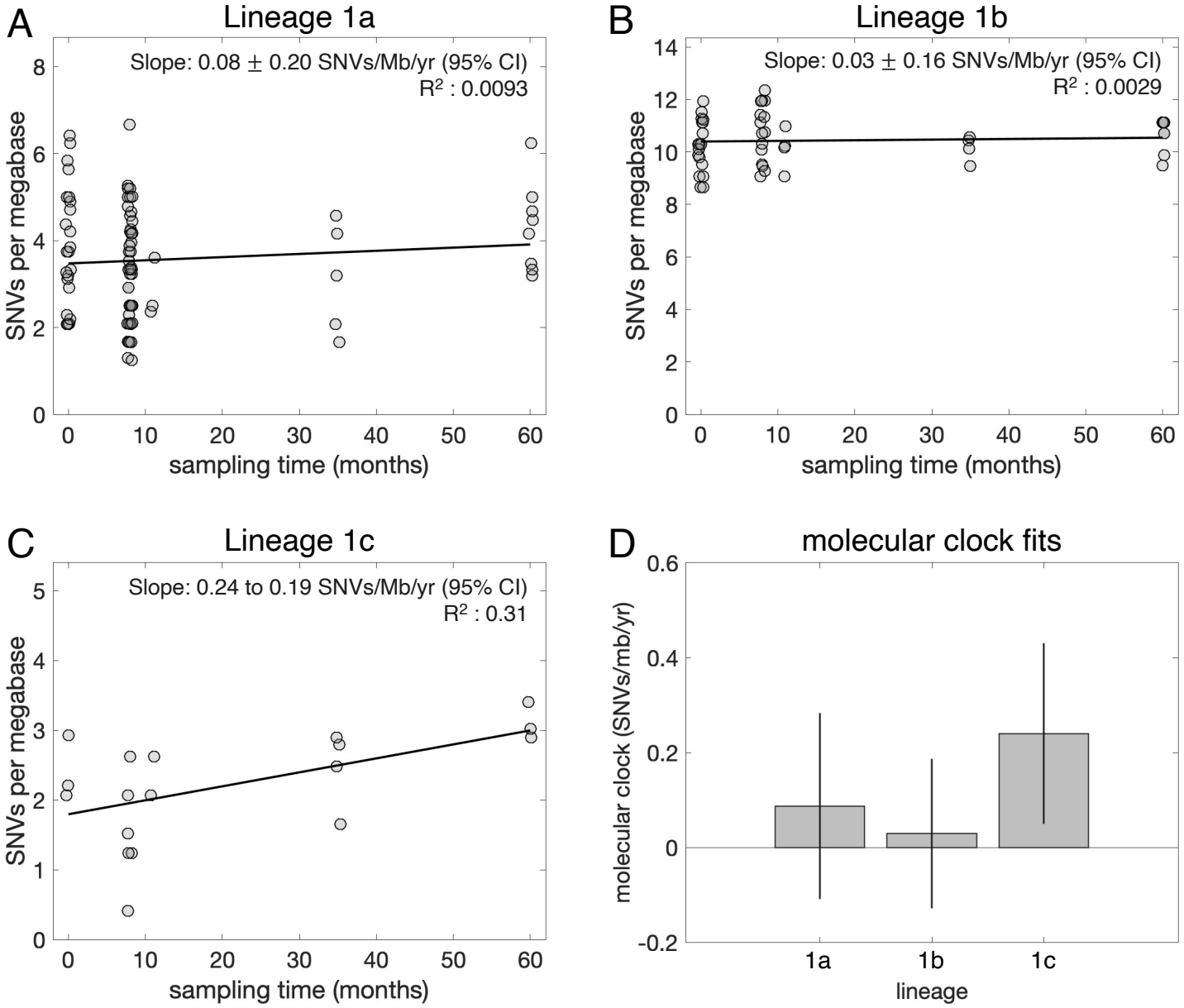

Figure S10. A molecular clock for *C. acnes* evolution is not detectable over a 5-year time course, related to Figure 5. We looked for a molecular clock signal in each of the three most abundant lineages on Subject 1, who was sampled longitudinally over five years. For each colony, we calculated the average number of mutations (SNVs) per 1 million base pairs (Mb) with sufficient coverage. We then averaged across colonies from a given sample, to account for the fact that colonies from the same sample are not independent. To assess the signal for mutation accumulation over time, we performed a linear regression between these sample averages and the time at which each sample was collected (note that some jitter is included in the time values displayed in the plots so that the point corresponding to each sample is visible). Fits for each lineage are shown in (A-C) and summarized in (D). We find no signal for a molecular clock within Lineages 1a and 1b, as indicated by a low r^2 value as well as by the 95% confidence interval of the slope including zero. This absence of a molecular clock signal suggests that the molecular clock for *C. acnes* on human skin is slower than could be captured by the length of the available time course or that either mutations/generation or generations/year are highly variable. For Lineage 1c, we find a detectable molecular clock signal of about 0.24 SNVs per megabase per year. While this value is consistent with values of molecular clocks from other species (Didelot et al., 2016), we opted not to convert numbers of mutations into amounts of time given the lack of signal in Lineages 1a and 1b.

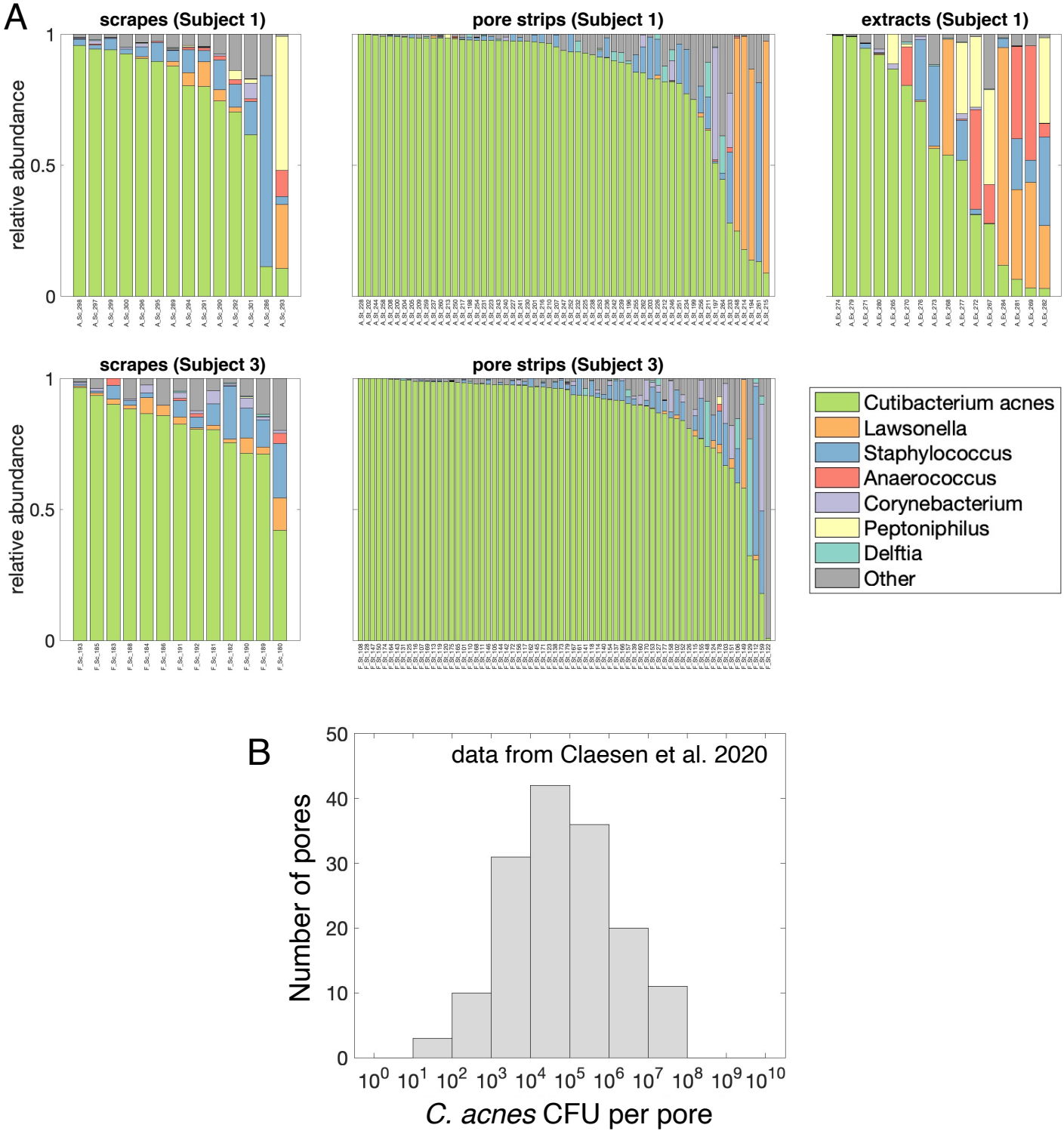

Figure S11. *C. acnes* dominates within-pore bacterial populations, related to Figure 5. (A) A subset of samples from two subjects was analyzed for community composition via 16S rRNA amplicon sequencing, in addition to colony-based *C. acnes* whole-genome sequencing (see Methods). Each species is colored in if its mean relative abundance across samples is >5% and each genus is colored if its max relative abundance across samples is >33%; everything else is categorized as "Other". Samples are categorized by collection method and subject. (B) Estimates of absolute abundances of *C. acnes* within individual pores derived from (Claesen et al., 2020). These estimates also agree with more limited data from our lab (data not shown).

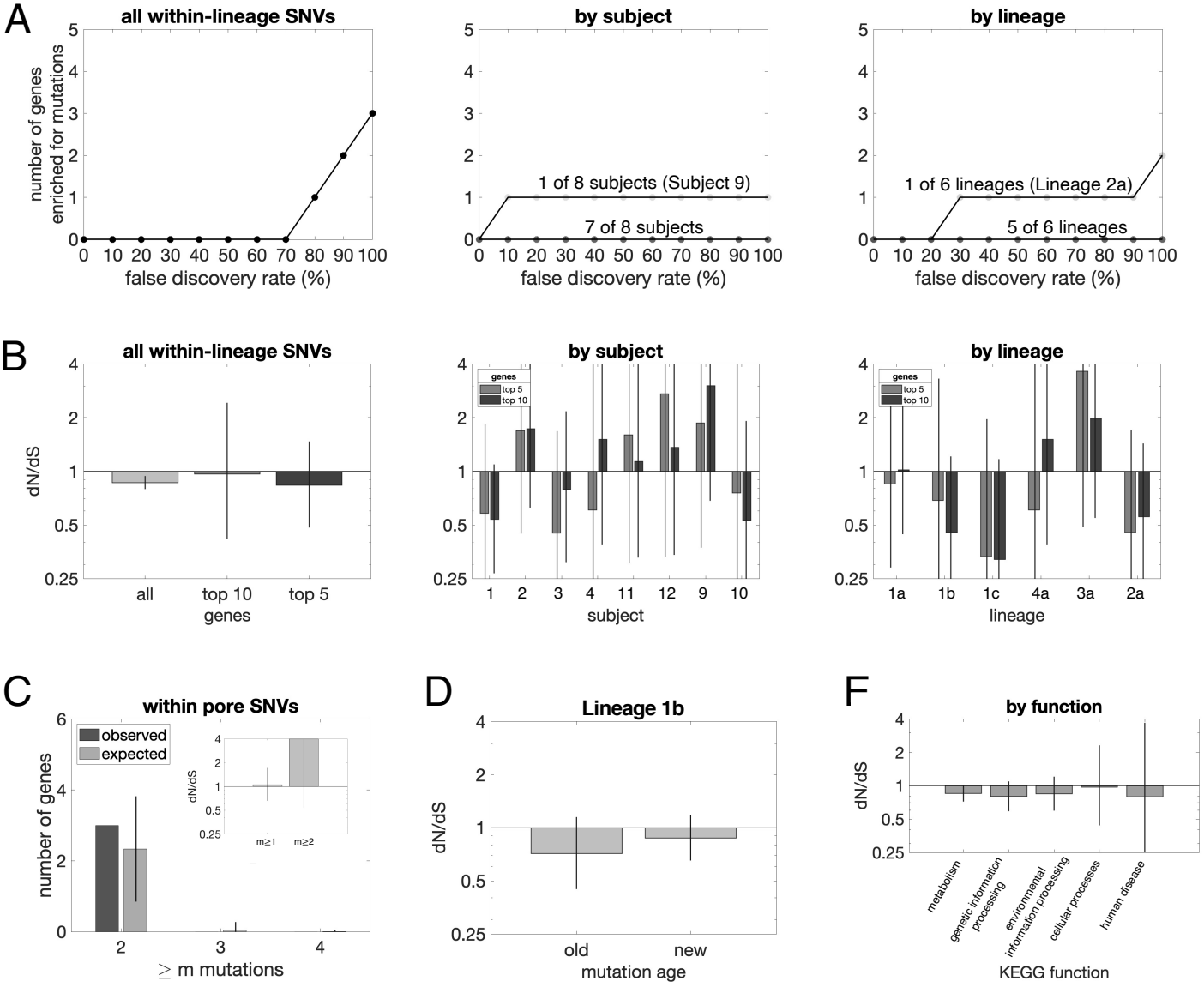

Figure S12. No evidence of parallel evolution among *de novo* SNPs, related to Figure 5. (A) In order to search for parallel evolution, we calculated p-values for mutational enrichment for each gene (Methods) and performed the Benjamini-Hochberg procedure to correct for multiple hypothesis testing (treating each gene on the genome as a hypothesis). We plotted the number of genes detected for a range of FDRs for (i) the set of all observed *de novo* mutations, (ii) all subjects with at least 100 *de novo* mutations, and (iii) all lineages with at least 100 *de novo* mutations. We find two cases in which a gene is found with an FDR below 50%--an M18-family aminopeptidase on Subject 9 and a carbohydrate ABC transporter permease in Lineage 2a (each with 2 nonsynonymous mutations and 1 synonymous mutation, consistent with a neutral model). (B-E) We calculated dN/dS as in Figure 5B (Methods), but for different sets of mutations. (B) shows dN/dS for the top 10 and top 5 most mutated genes (according to Poisson p-values) across all mutations, by subject, and by lineage. (C) shows dN/dS for mutations inferred to have occurred inside pores (no parallel evolution detected with the Benjamini-Hochberg procedure; no enrichment of genes mutated multiple times relative to a neutral model; and no significant enrichment of nonsynonymous mutations on genes with multiple mutations, P=0.1); (D) shows dN/dS for older mutations on the long branches of Lineage 1b is not significantly different than newer mutations in the Lineage 1b subclades (Figure S7); and (E) shows dN/dS by KEGG function. Error bars represent 95% confidence intervals, demonstrating no significant signature for adaptive evolution.

A

$$\frac{\partial n}{\partial t} = D\frac{\partial^2 n}{\partial x^2} - v\frac{\partial n}{\partial x}$$

Drift-Diffusion equation where $n(x,t)$ is the probability that the cell is at pore depth x at time t, with reflecting boundary conditions at the bottom of the pore ($x = 1000\mu m$) and absorbing boundary conditions at the top of the pore ($x = 0\mu m$)

B

Parameter	Value	Source
Diffusion coefficient (*D*) of a cell in sebum	650 μm²/day	Stokes-Einstein equation ($D = \frac{k_B T}{6\pi\eta r}$) • Boltzmann constant k_B • Body temperature $T = 37\text{C}$ • Sebum viscosity $\eta = 600$ millipoises (Butcher et al., 1949) • Cell radius $r = 0.5$ μm
Sebum flow speed (*v*) upward in the pore	-50 μm/day	Estimated from time for an extracted sebaceous follicle to refill (20 days) reported by (Plewig, 1974) for a pore of depth 1 mm
C. acnes doubling time (t_g)	0.5 days	Estimated from max growth rates of *C. acnes* in laboratory aerobic conditions reported by (Cove et al.,1983)

C

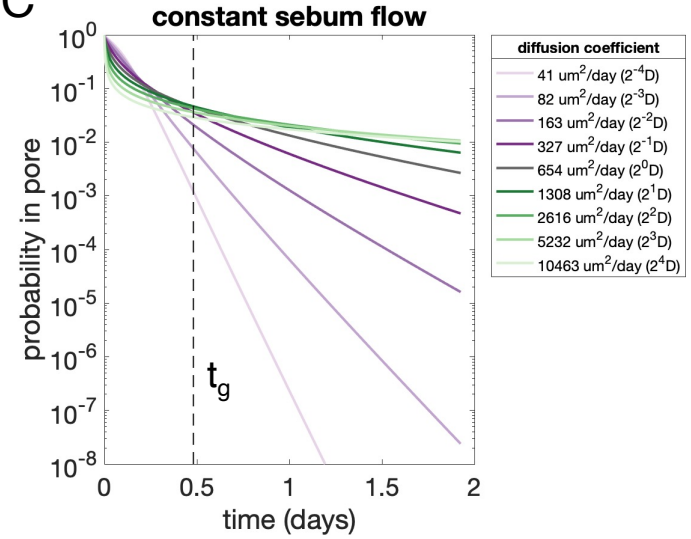

D

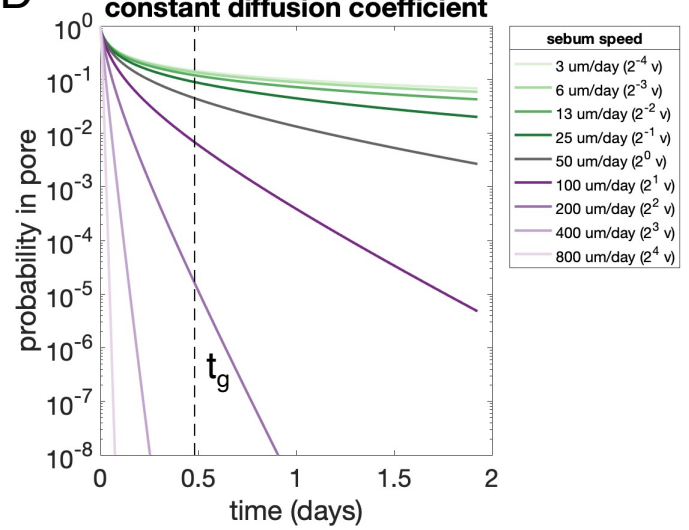

Figure S13. Pore physiology may be responsible for neutral bottlenecking, related to Figure 5. Individual cells attempting to colonize pores have a low likelihood of successfully colonizing a pore under reasonable assumptions. We modeled the diffusion of a cell through sebum as indicated in (A) and using conservative parameters estimated in (B), which are likely to overestimate the probability of a cell remaining in the pore, as a starting point. This model was implemented in Matlab (v2018a). (C-D) We explored 2^4-fold variation in either direction of the diffusion coefficient *D* and the sebum speed *v*, and we calculated the probability of a cell of a single cell remaining within the pore as a function of time. We assumed that a cell starts (at *t*=0) within in the top 10 um of the pore. (C-D) show how the probabilities change (C) for different diffusion coefficients and (D) for different rates of sebum flow. These probabilities are particular sensitive to sebum flow rate. While the number of cells attempting to colonize a pore at a given time is unknown, these low likelihoods of successful colonization provide many generations during which a single-cell colonizer can expand to dominate the pore before the next successful colonization event. In addition, a cell that reaches the lower depths of the pore will have an advantage over later colonizers because of the anaerobic environment. Moreover, diffusion will likely be substantially slower due in a partially or fully colonized pore, where cells that are already in the pore create obstacles to other cells—making it even more difficult for a new colonizer to penetrate deeper into the pore.

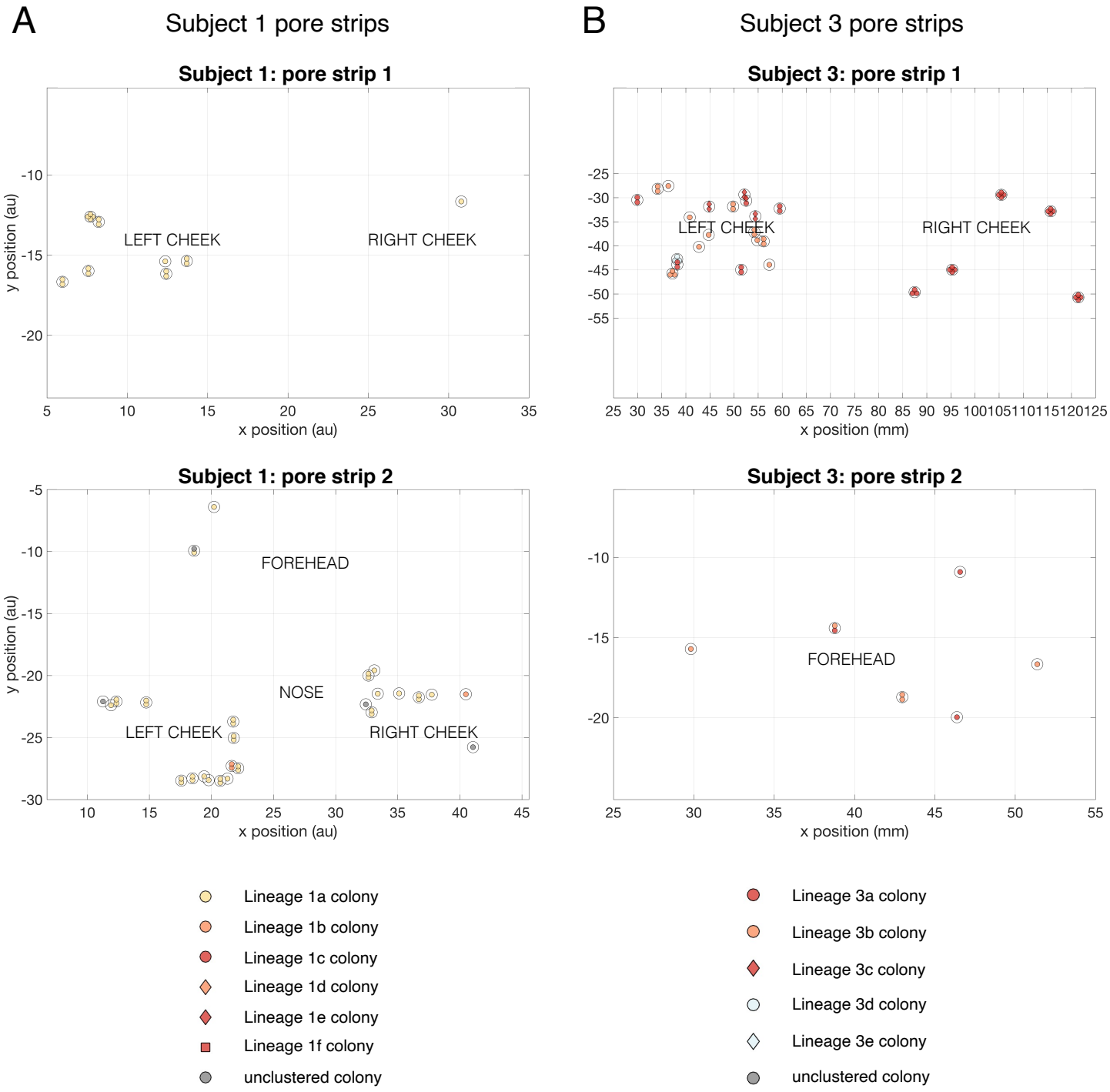

Figure S14. Spatial coordinates and lineages for pore strip colonies, related to Figures 3 and 5. Pore strip samples from Subject 1 (A) and Subject 3 (B) enabled us to collect colonies from pores with defined spatial coordinates. Each sample derived from a single follicle is denoted by an open circle. Each colony from that sample is represented by a symbol inside that circle, where the color represents the strain type (same color scheme as Figures 2, 3, and S4) and the shape represents the lineage. Approximate facial regions are marked with text labels. Lineages are ordered by abundance across all colonies from the subject (even if that lineage was not represented in pore strip colonies).

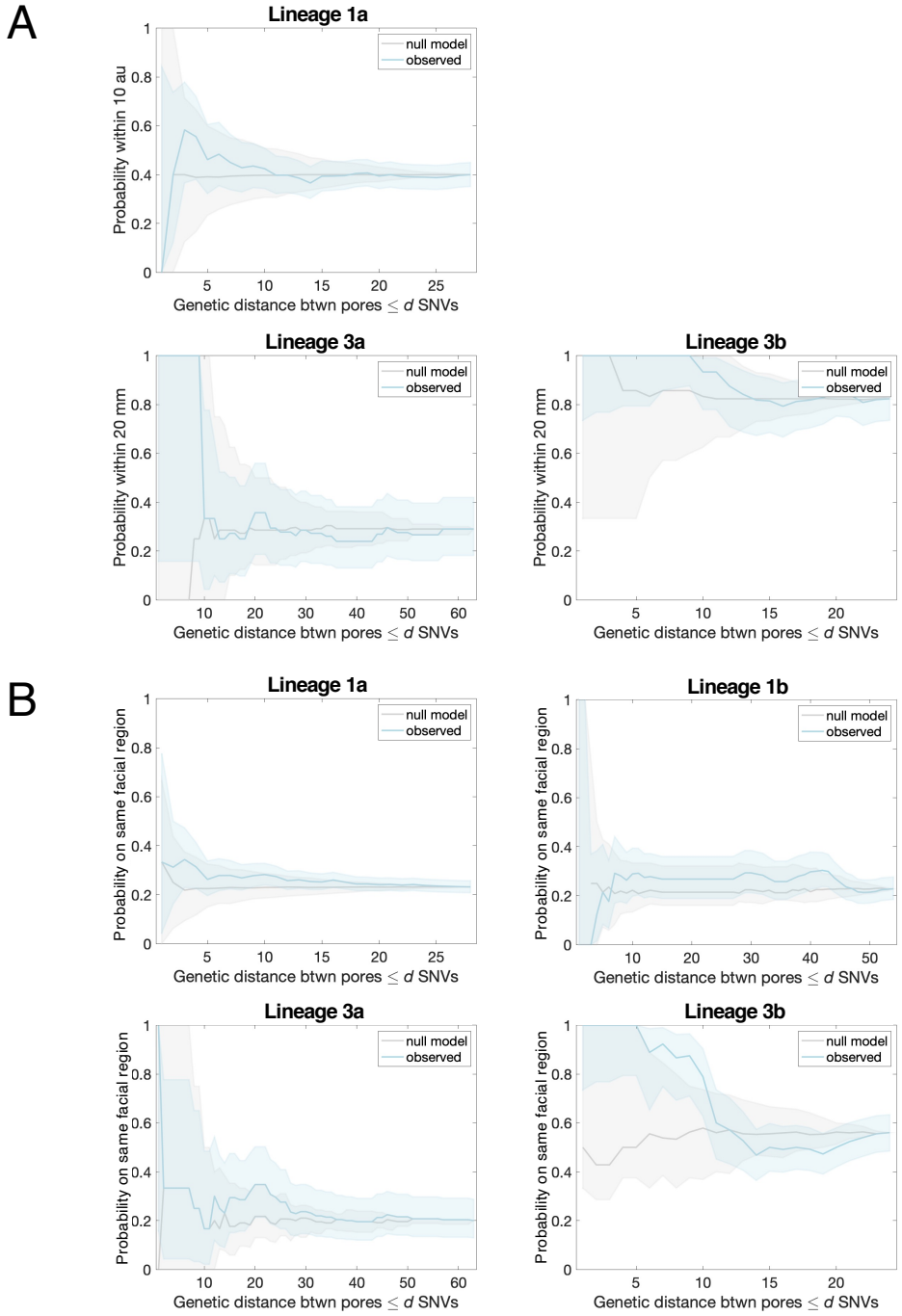

Figure S15. Lineages spread across the face faster than they accumulate mutations, related to Figure 5. (A) In order to determine if physical distance between pores was related to genetic distance between pores, we computed the the probability that pairs of pores harboring colonies from the same lineage within *d* SNVs of each other were co-localized (within 20 mm for Subject 3; within 10 arbitrary units for Subject 1, which is approximately equivalent to 20 mm). We compared this probability to that expected from a null model, where the spatial coordinates of pores were re-shuffled. Plots show 95% CIs (binomial distribution). Only pore sample originating from a single follicle and whose colonies were monophyletic were used in this analysis, so that we could compute the genetic distance between pores as the number of SNVs between inferred pore ancestors (Methods); lineages with at least 10 pores with spatial coordinates are included. (B) We repeated this analysis including colonies from pore extracts subject to the same criteria as noted above, computing the probability that genetically related pairs of pores were confined to the same facial skin region (see Figure 3). In both cases, we did not detect spatial confinement, suggesting that lineages spread across the face faster than they accumulate mutations.

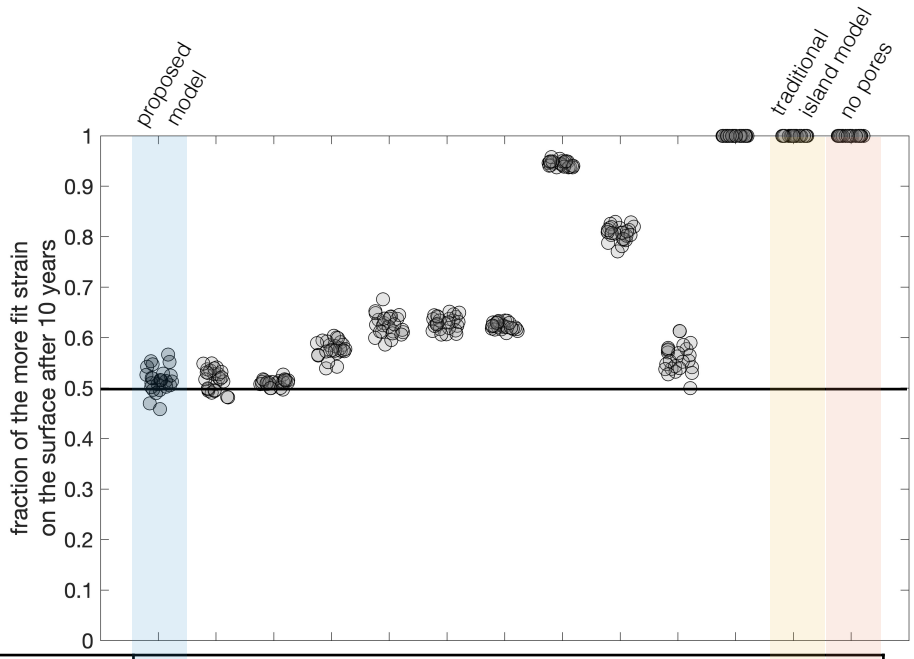

Parameters that do change	Values												
Number of cells that initially colonize a pore follicle	1	2	10	1	1	2	10	1	1	1	2	1	n/a
Migration post-colonization (fraction of cells in a pore replaced by cells from the surface each day)	0	0	0	.01	0	0	0	.01	0	0	0	.01	n/a
Doubling time of cells of the less fit strain in pores (days)	30	30	30	30	3	3	3	3	1	30	30	30	n/a
Fitness advantage of the more fit strain inside pores (0% if growth is limited by sebum production)	0%	0%	0%	0%	0%	0%	0%	0%	0%	0%	50%	50%	n/a
Doubling time of cells of the less fit strain on the surface (days)	150	150	150	150	15	15	15	15	5	30	150	30	30

Parameters that differ from our proposed model are highlighted in gray.

Figure S16. Competition model recapitulates how pores play a key role in lineage coexistence, related to Figure 5. We used a mathematical model (Methods) to explore how different processes on skin might shift competitive outcomes between two strains, one of which has a large fitness advantage. For each model tested, we ran 25 independent simulations, and the competitive outcomes are summarized above along with the parameter values for each model (parameters that are the same across all simulations are listed to the right). Our proposed model (blue) of skin dynamics, and includes strong population bottlenecking upon pore colonization, and cell growth inside pores that is limited by sebum production (resulting in no fitness differences); this results in minimal competition over a simulation of 10 years. In contrast, a traditional island model (yellow) that allows for competition in pores ("islands") and for migration from the surface ("mainland") into colonized pores would not limit competition. Similarly, a model with no pores (surface population only) would also allow the more fit strain to take over the population rapidly. These results emphasize how features inherent to pores can severely limit inter-strain competition on an individual.

Parameters that do not change	Value
Number of pores	10,000
Migration out of pores (fraction of cells on the surface replaced by cells from pores each day)	1/3
Average frequency of pore re-colonization events	10,000/ year
Fitness advantage of the more fit strain on the surface	50%
Initial population fraction of the fitter strain	0.5

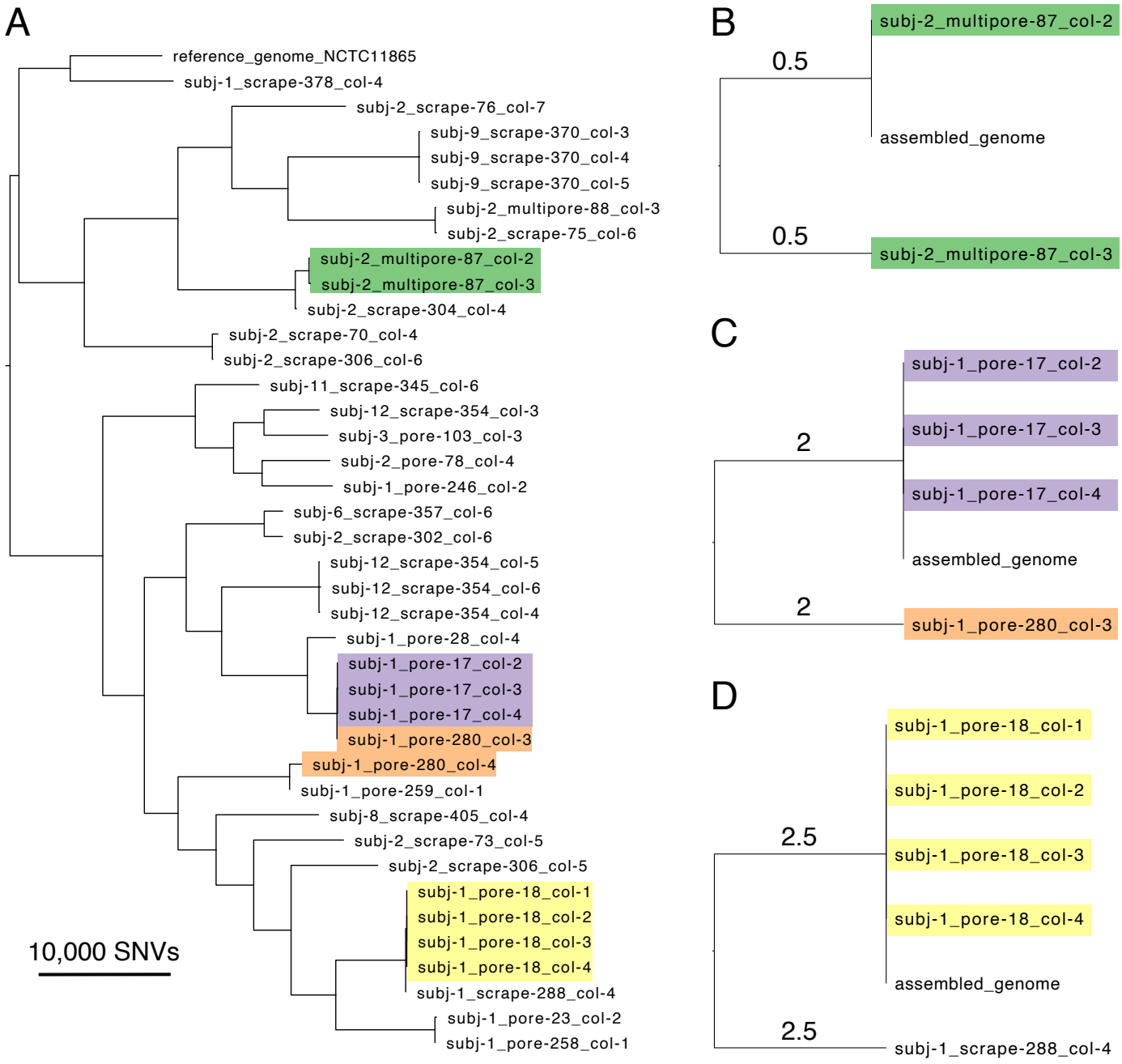

Figure S17. Limited genetic diversity among *Cutibacterium granulosum* colonies originating from the same pore, related to Figure 4. While aiming to sequence *C. acnes* colonies, we sometimes cultured colonies of other species, and 50 colonies were identified as *C. granulosum*. (A) SNVs were analyzed using an alignment-based approach to reference genome NCTC11865 and evolutionary reconstruction was performed, using a similar approach as for *C. acnes* (Methods). Maximum parsimony of the 39 *C. granulosum* colonies that passed quality filtering shows the presence of distinct lineages on each person. Note that genetic distances are approximate, as no effort was made to distinguish variable gene content or recombination from SNVs. Cases where multiple colonies originate from the same pore sample are highlighted. (B-D) In order to investigate the within-pore diversity at a finer scale, we assembled genomes for each of the three cases where colonies from the same pore were monophyletic and repeated evolutionary reconstruction (Methods). Branch lengths are annotated in SNVs. These trees show that *C. granulosum* colonies from the same pore share nearly identical genomes. (A-D) All trees are midpoint rooted.